J. Appl. Comput. Mech., 5(2) (2019) 281-298
DOI: 10.22055/JACM.2018.25177.1237

ISSN: 2383-4536
jacm.scu.ac.ir

M&MoCS

Shahid Chamran University of Ahvaz

Journal of Applied and Computational Mechanics

Research Paper

Bending and Free Vibration Analysis of Functionally Graded Plates via Optimized Non-polynomial Higher Order Theories

D.A. Ramirez[1], L.M. Cuba[2], J.L. Mantari[1,3], R.A. Arciniega[2]

[1] Faculty of Mechanical Engineering, National University of Engineering (UNI), Av. Túpac Amaru 210, Rimac, Lima, Peru
[2] Department of Civil Engineering, Universidad Peruana de Ciencias Aplicadas (UPC), Lima, Peru
[3] Faculty of Mechanical Engineering, Universidad de Ingeniería y Tecnología (UTEC), Jr. Medrano Silva 165, Barranco, Lima, Peru

Received March 02 2018; Revised September 08 2018; Accepted for publication September 14 2018.
Corresponding author: J.L. Mantari, jmantari@utec.edu.pe

Abstract. Optimization concept in the context of shear deformation theories was born for the development of accurate models to study the bending problem of structures. The present study seeks to extend such an approach to the dynamic analysis of plates. A compact and unified formulation with non-polynomial shear strain shape functions (SSSFs) is employed to develop a static and free vibration analysis of simply supported functionally graded plates. In this context, three new non-polynomial displacement fields are proposed using trigonometric and hyperbolic SSSFs. Then, the non-polynomial SSSFs are optimized by varying the arguments of the trigonometric and hyperbolic functions. Additionally, the Mori-Tanaka approach is used to estimate the effective properties of the functionally graded plates. The Principle of Virtual Displacement (PVD) and the Hamilton's Principle along with the Navier closed-form solution technique are used to obtain exact results. The obtained numerical results are in a good agreement with 3D and 2D higher order shear deformation theory solutions available in the literature.

Keywords: Static analysis; Free vibration; Shear strain shape function; Functionally graded materials; Unified formulation.

1. Introduction

Laminated composites are gaining more and more protagonist as a solution to engineering applications in which classic materials are not able to satisfy stiffness and strength requirements. Some of these applications are commonly found in nuclear reactors as well as aircraft, spacecraft, biomechanical, shipbuilding, and other industries. However, laminated composites suffer from discontinuity at layer interfaces producing several challenging problems to solve up to date, one of which can be the initiation of cracks or the presence of residual stresses produced by the difference in the thermal coefficient at layer interfaces. Functionally graded materials (FGMs), initially proposed by Bever and Duwez [1], can be a solution to avoid such mechanical problems.

The functionally graded materials (FGMs) could be defined as a composite in which the material properties are gradually varied along a certain direction as a function of the position coordinates to achieve desired strength and stiffness. In a typical functionally graded plate, the material properties continuously vary over the thickness direction by mixing two different materials. Additionally, there are many ways to fabricate FGMs, for instance Miyamoto et al. [2] and Kieback [3] suggest some of the most common production methods.

So far, several research works were performed to study the behavior of FG beams, shells, and plates. In particular, Swaminathan et al. [4] presented an interesting review on the static, vibration, and buckling analysis of FG plates. The study of such mechanical problems can be performed using analytical or numerical methods. A starting point for the analytical methods in vibration analysis was introduced by Reddy and Cheng [5]. They developed a three-dimensional (3D) asymptotic theory formulated in terms of the transfer matrix. Moreover, Vel and Batra [6] carried out a three-dimensional exact solution for the

Published online: February 09 2019

free and forced vibration of a simply supported FG rectangular plate using the power series expansion method and Mori-Tanaka technique to homogenize material properties [7-8]. Interestingly, it was found that the outcomes obtained from the first order shear deformation theory (FSDT) perform better than the third order shear deformation theory (TSDT), and the classic plate theory (CPT) provides unreliable results. In fact, the analytical methods based on 3D elasticity theories are the most accurate techniques to solve static and dynamic problems, therefore, their results are considered as benchmarks for studies conducted based on two-dimensional (2D) analytical and numerical methods.

Additionally, other research works were presented to address dynamic problems of FG plates by employing analytical methods and using 2D elasticity theory. For example, Zenkour [9] proposed trigonometric series representation through the plate thickness to express displacement components of simply supported FG thick plates. Zenkour [10, 11] employed a sinusoidal shear deformation plate theory (SSDT) to analyze bending, vibration, and buckling behavior of the simply supported FG sandwich plate. In addition, Matsunaga [12] developed a buckling and free vibration analysis of FG plates by taking into account the effects of transverse shear and normal deformations along with rotatory inertia. Fares et al. [13] handed over a refined equivalent single-layer (ESL) shear deformation theory for an orthotropic FG plate by a modified version of mixed variational principle of Reissner (RMVT). Likewise, Cinefra et al. [14], using the RMVT and Carrera Unified Formulation (CUF), performed a dynamic analysis of FG shells. Lastly, Hadji et al. [15] used Shimpi's four variable refined plate theory for the free vibration analysis of FG sandwich plates, concluding that the notwithstanding refined plate theory is simple and able to predict accurate outcomes.

On the other hand, numerical methods were extensively used to analyze bending, vibration, and buckling of FG plates. Qian and Batra [16] performed a free and forced vibration analysis using high-order shear deformation theories (HSDTs) and meshless local Petrov–Galerkin (MLPG) method. Besides, the global collocation method along with the FSDT and TSDT, and Mori-Tanaka approach were employed by Ferreira et al. [17] in order to find the natural frequencies of FG plates. Neves et al. [18-19] used the principle of virtual displacements (PVD) under CUF and a meshless technique based on the collocation with radial basis functions to address the thickness stretching issue on the static, free vibration, and buckling analysis of FG plates by employing a quasi-3D SSDT [18] and a quasi-3D HSDT [19].

Likewise, using PVD and CUF to obtain both closed-form and finite element (FE) solutions, Carrera and Brischetto [20] addressed the static analysis of functionally graded plates subjected to transverse mechanical loadings using FSDT and HSDT. Carrera et al. [21] presented results using RMVT for bending analysis of FG plate by considering both displacements and transverse shear/normal stresses as primary variables. In addition, Carrera et al. [22] considered the effect of transverse normal strain in FG plates and shells. Mantari et al. [23-26] proposed a normal and optimized HSDT solution using Navier's solution to get closed to 3D solution by properly selecting the arguments of the proposed SSSFs. Overall, several shear deformation theories can be evaluated by the compact and unified formulation as described in this section, and it is possible to have at one glance their performance. However, few researchers were concerned with theories that consider both non-polynomial shear strain functions and low number unknown variables at the same time, which is addressed in the present study.

The aim of the current research is to extend the work performed by Mantari et al. [26] which is related to the bending analysis and investigate the static and free vibration of advanced composites by employing an optimization process to obtain the most accurate outcomes for the eigenvalue problem of a simply supported FG rectangular plate. The present formulation follows the compactness presented by the Carrera's Unified Formulation (CUF) along with the Principle of Virtual Work (PVD) and the Hamilton Principle to find the governing equations. The static and dynamic problem is solved by the closed-form Navier's solution. Furthermore, three non-polynomial displacement fields are proposed. The obtained results demonstrate that the optimized HSDTs shows a good agreement with respect to the 3D elasticity solution by performing a proper selection of the arguments of the non-polynomial SSSFs.

2. Analytical Modelling

The static analysis of the present research has been developed using a rectangular FG plate made of Aluminium (Al) and Alumina (Al_2O_3). For the vibration analysis, a FG plate made of Aluminium and Zirconia (ZrO_2) is considered. In both cases, different values of p = {1, 2, 3, 5} are taken into consideration. Moreover, Table 1 provides the mechanical properties of the constituents.

2.1. Functionally graded plates

Consider a single rectangular plate with the uniform thickness "*h*", length "*a*", and wide "*b*" (see Fig.1). The middle plane of the plate has been chosen as the plane *xy* of the Cartesian coordinate system while X-axis and Y-axis parallels to edges of the plate. The plate is made of a FGM having two distributed isotropic constituents. In addition, it is assumed that the Volume fraction of one of the plate constituents follows the powder law distribution as:

$$V_{2(z)} = V_2{}^- + (V_2{}^+ - V_2{}^-)\left(\frac{z}{h}+\frac{1}{2}\right)^p, \qquad -\frac{h}{2} \le z \le \frac{h}{2} \tag{1}$$

Table 1. Material properties of FG plate.

Material	Properties		
	E (GPa)	ν	ρ (kg/m^3)
Aluminium (Al)	70	0.3	2702
Alumina (Al2O3)	380	0.3	3800
Zirconia (ZrO2)	200	0.3	5700

Therefore, V_2^- and V_2^+ denotes the volume fraction related to the faces of the plate, bottom and top, respectively. Additionally, the exponent "*p*" provides the material variation profile through the thickness (See Fig. 2).

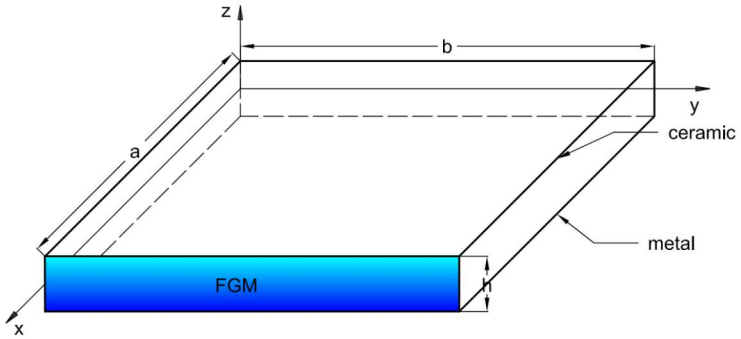

Fig. 1. Geometry of functionally graded single plate

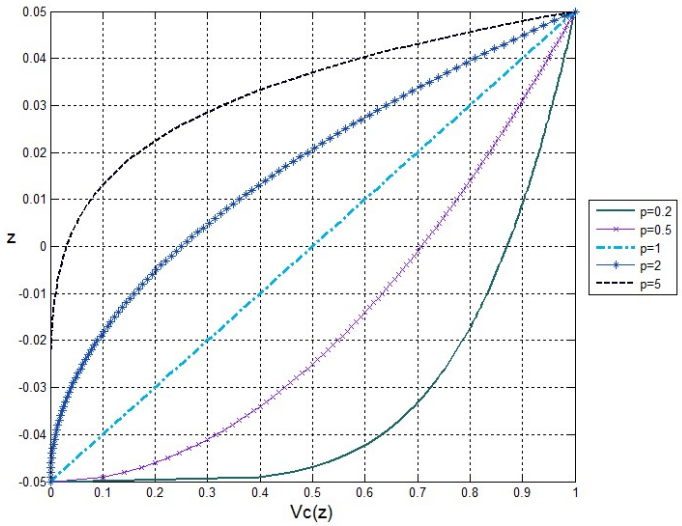

Fig. 2. Functionally graded function Vc along the thickness of a FG plate (Al/Al_2O_3) for a set of values of "p".

According to the law-of-mixture, the properties of the plate are calculated as follows:

$$P_{(z)} = (P_2 - P_1) \times V_{2(z)} + P_1 \tag{2}$$

where, P denotes a material property such as Young's Modulus (E), Shear Modulus (G), density (ρ) and so on.

Moreover, the Mori-Tanaka homogenization method is used to estimate the effective bulk modulus "$\boldsymbol{K}$" and the effective shear modulus $\boldsymbol{G}$ by using the following equations:

$$\frac{K - K_1}{K_2 - K_1} = \frac{V_2}{1 + (1 - V_2)\dfrac{K_2 - K_1}{K_1 - \dfrac{4}{3}G_1}} \tag{3a}$$

$$\frac{G - G_1}{G_2 - G_1} = \frac{V_2}{1 + (1 - V_2)\dfrac{G_2 - G_1}{G_1 - f_1}} \tag{3b}$$

where $f_1 = \frac{(9K_1+8G_1)G_1}{6(K_1+2G_1)}$. Therefore, the effective Young's modulus "$\boldsymbol{E}$" and Poisson's ratio "$\boldsymbol{\nu}$" are calculated using the following equations:

$$E = \frac{9KG}{3K + G} \tag{4a}$$

$$\nu = \frac{3K - 2G}{2(3K + G)} \tag{4b}$$

2.2. Displacement based field

For an Equivalent Single Layer (ESL) plate, the Carrera's Unified Formulation assumes the following form of the displacement field:

$$\boldsymbol{u} = F_\tau u_\tau \qquad \tau = 0,1,2 \ldots . N \tag{5a}$$

where, F_τ depends on z and u_τ is a function of x, y, and time t. In this study, for the optimizing procedure, F_τ is assumed to be:

$$F_\tau = \begin{bmatrix} F_{m,\tau} & 0 & 0 \\ 0 & F_{m,\tau} & 0 \\ 0 & 0 & F_{n,\tau} \end{bmatrix} \tag{5b}$$

and

$$u_\tau = \begin{bmatrix} u_{x,\tau} \\ u_{y,\tau} \\ u_{z,\tau} \end{bmatrix} \tag{5c}$$

Using the Einstein notation,

$$u_\tau = F_{m,\tau} \times u_{x,\tau} \tag{6}$$

In expanded form,

$$\begin{aligned} \boldsymbol{u_x}(x,y,z,t) &= F_{m,0}u_{x0} + F_{m,1}u_{x1} + F_{m,2}u_{x2} + F_{m,3}u_{x3} + \cdots \\ \boldsymbol{u_y}(x,y,z,t) &= F_{m,0}u_{y0} + F_{m,1}u_{y1} + F_{m,2}u_{y2} + F_{m,3}u_{y3} + \cdots \\ \boldsymbol{u_z}(x,y,z,t) &= F_{n,0}u_{z0} + F_{n,1}u_{z1} + F_{n,2}u_{z2} + F_{n,3}u_{z3} + \cdots \end{aligned} \tag{7a-c}$$

where $F_{m,i}$, $F_{n,i}$ are non-polynomial functions of z and *m* and *n* refer to the SSSF arguments, respectively. The SSSFs are of trigonometrical and hyperbolic in nature.

2.3. Elastic stress-strain relation

Employing CUF, the stresses (σ^K) and strains (ϵ^K) can be grouped as follows:

$$\begin{aligned} {\sigma_p}^K &= \begin{bmatrix} {\sigma_{xx}}^K & {\sigma_{yy}}^K & {\sigma_{xy}}^K \end{bmatrix}^T \\ {\sigma_n}^K &= \begin{bmatrix} {\sigma_{xz}}^K & {\sigma_{zy}}^K & {\sigma_{zz}}^K \end{bmatrix}^T \\ {\epsilon_p}^K &= \begin{bmatrix} {\epsilon_{xx}}^K & {\epsilon_{yy}}^K & {\epsilon_{xy}}^K \end{bmatrix}^T \\ {\epsilon_n}^K &= \begin{bmatrix} {\epsilon_{xz}}^K & {\epsilon_{zy}}^K & {\epsilon_{zz}}^K \end{bmatrix}^T \end{aligned} \tag{8a-d}$$

where *k-th* represent layers, the subscript *n* means in-plane components, and *p* means out-of-plane components. Assuming a normal or lineal strain,

$$\begin{aligned} \boldsymbol{\varepsilon}_p^k &= \boldsymbol{D}_p \boldsymbol{u}^k \\ \boldsymbol{\varepsilon}_n^k &= \boldsymbol{D}_n \boldsymbol{u}^k = \left(\boldsymbol{D}_{np} + \boldsymbol{D}_{nz}\right)\boldsymbol{u}^k \end{aligned} \tag{9a-b}$$

Therefore,

$$\boldsymbol{D}_p = \begin{bmatrix} \frac{\partial}{\partial x} & 0 & 0 \\ 0 & \frac{\partial}{\partial y} & 0 \\ \frac{\partial}{\partial y} & \frac{\partial}{\partial x} & 0 \end{bmatrix}, \quad \boldsymbol{D}_{np} = \begin{bmatrix} 0 & 0 & \frac{\partial}{\partial x} \\ 0 & 0 & \frac{\partial}{\partial y} \\ 0 & 0 & 0 \end{bmatrix}, \quad \boldsymbol{D}_{nz} = \begin{bmatrix} \frac{\partial}{\partial z} & 0 & 0 \\ 0 & \frac{\partial}{\partial z} & 0 \\ 0 & 0 & \frac{\partial}{\partial z} \end{bmatrix} \tag{10a-c}$$

Moreover, Hooke's law provides the stress-strain relationship as

$$\boldsymbol{\sigma}^K = \boldsymbol{C}^K \boldsymbol{\epsilon}^K \tag{11a}$$

$$\begin{bmatrix} \sigma_{xx}^k \\ \sigma_{yy}^k \\ \sigma_{xy}^k \\ \sigma_{xz}^k \\ \sigma_{yz}^k \\ \sigma_{zz}^k \end{bmatrix} = \begin{bmatrix} C_{11}^k(z) & C_{12}^k(z) & 0 & 0 & 0 & C_{13}^k(z) \\ C_{12}^k(z) & C_{22}^k(z) & 0 & 0 & 0 & C_{23}^k(z) \\ 0 & 0 & C_{66}^k(z) & 0 & 0 & 0) \\ 0 & 0 & 0 & C_{55}^k(z) & 0 & 0 \\ 0 & 0 & 0 & 0 & C_{44}^k(z) & 0 \\ C_{13}^k(z) & C_{23}^k(z) & 0 & 0 & 0 & C_{33}^k(z) \end{bmatrix} \begin{bmatrix} \varepsilon_{xx}^k \\ \varepsilon_{yy}^k \\ \varepsilon_{xy}^k \\ \varepsilon_{xz}^k \\ \varepsilon_{yz}^k \\ \varepsilon_{zz}^k \end{bmatrix} \tag{11b}$$

The components C_{ij}^k of the matrix $\boldsymbol{C}^K$ are given as follows:

$$C_{11}^k(z) = C_{22}^k(z) = C_{33}^k(z) = \frac{E(z)\,(1-\nu)}{(1-2\nu)(1+\nu)}$$
$$C_{13}^k(z) = C_{23}^k(z) = C_{12}^k(z) = \frac{E(z)\,\nu}{(1-2\nu)(1+\nu)} \tag{12a-c}$$
$$C_{55}^k(z) = C_{44}^k(z) = C_{66}^k(z) = \frac{E(z)}{2(1+\nu)}$$

According to Eq. (11a), Eqs. (8a-b) can be rewritten as:

$$\boldsymbol{\sigma}_p^k = \left(\boldsymbol{C}_{pp}^k \boldsymbol{\varepsilon}_p^k + \boldsymbol{C}_{pn}^k \boldsymbol{\varepsilon}_n^k\right)$$
$$\boldsymbol{\sigma}_n^k = \left(\boldsymbol{C}_{np}^k \boldsymbol{\varepsilon}_p^k + \boldsymbol{C}_{nn}^k \boldsymbol{\varepsilon}_n^k\right) \tag{13a-b}$$

where

$$\boldsymbol{C}_{pp}^k = \begin{bmatrix} C_{11(z)}^k & C_{12(z)}^k & 0 \\ C_{12(z)}^k & C_{22(z)}^k & 0 \\ 0 & 0 & C_{66(z)}^k \end{bmatrix}^k \quad \boldsymbol{C}_{nn}^k = \begin{bmatrix} C_{55(z)}^k & 0 & 0 \\ 0 & C_{44(z)}^k & 0 \\ 0 & 0 & C_{33(z)}^k \end{bmatrix}^k$$
$$\boldsymbol{C}_{np}^k = \begin{bmatrix} 0 & 0 & 0 \\ 0 & 0 & 0 \\ C_{13(z)}^k & C_{23(z)}^k & C_{36(z)}^k \end{bmatrix}^k \quad \boldsymbol{C}_{pn}^k = \begin{bmatrix} 0 & 0 & C_{13(z)}^k \\ 0 & 0 & C_{23(z)}^k \\ 0 & 0 & C_{36(z)}^k \end{bmatrix}^k \tag{14a-d}$$

2.4. Principle of virtual displacements

Hamilton's principle can be expressed as:

$$\delta \int_{t_1}^{t_2} (U + V_e - T)dt = 0 \tag{15}$$

where U is the strain energy, V_e is the potential energy of the elastic foundation, and T is the kinetic energy. Neglecting the potential energy, Eq. (15) can be rewritten as:

$$\sum_{k=1}^{N_l} \int_{\Omega_k} \int_{A_k} \left\{\delta \boldsymbol{\varepsilon}_p^{k\,T} \boldsymbol{\sigma}_p^k + \delta \boldsymbol{\varepsilon}_n^{k\,T} \boldsymbol{\sigma}_n^k\right\} d\Omega_k dz = \sum_{k=1}^{N_l} \int_{\Omega_k} \int_{A_k} \delta \boldsymbol{u}^k \boldsymbol{\rho} \ddot{\boldsymbol{u}}^k \, d\Omega_k dz \tag{16}$$

where $\boldsymbol{\varepsilon}_p^k$ or $\boldsymbol{\sigma}_p^k$ are the stress and the strain vectors of the *k-th* layer, N_l stands for the number of layers, and δL_{ine}^k is the external virtual work.

Using the previous equations in (16), it yields:

$$\int_{\Omega_k} \int_{A_k} \Big\{ \left(\boldsymbol{D}_p \delta \boldsymbol{u}^k\right)^T \left[\boldsymbol{C}_{pp}^k \boldsymbol{D}_p + \boldsymbol{C}_{pn}^k \left(\boldsymbol{D}_{np} + \boldsymbol{D}_{nz}\right)\right] \boldsymbol{u}^k$$
$$+ \left(\left(\boldsymbol{D}_{np} + \boldsymbol{D}_{nz}\right)\delta \boldsymbol{u}^k\right)^T \left[\boldsymbol{C}_{np}^k \boldsymbol{D}_p + \boldsymbol{C}_{nn}^k \left(\boldsymbol{D}_{np} + \boldsymbol{D}_{nz}\right)\right] \boldsymbol{u}^k \Big\} d\Omega_k dz \tag{17}$$
$$= \sum_{k=1}^{N_l} \int_{\Omega_k} \int_{A_k} \delta \boldsymbol{u}^k \boldsymbol{\rho} \ddot{\boldsymbol{u}}^k \, d\Omega_k dz$$

Moreover, considering Eq. (5a), Eq. (17) becomes:

$$\int_{\Omega_k} \int_{A_k} \Big\{ \left(\boldsymbol{D}_p \boldsymbol{F}_\tau \delta \boldsymbol{u}_\tau{}^k\right)^T \left[\boldsymbol{C}_{pp}^k \boldsymbol{D}_p \boldsymbol{F}_S \boldsymbol{u}_S{}^k + \boldsymbol{C}_{pn}^k \boldsymbol{D}_{np} \boldsymbol{F}_S \boldsymbol{u}_S{}^k + \boldsymbol{C}_{pn}^k \boldsymbol{F}_{S,z} \boldsymbol{u}_S{}^k\right]$$
$$+ \left(\boldsymbol{D}_{np} \boldsymbol{F}_\tau \delta \boldsymbol{u}_\tau{}^k\right)^T \left[\boldsymbol{C}_{np}^k \boldsymbol{D}_p \boldsymbol{F}_S \boldsymbol{u}_S{}^k + \boldsymbol{C}_{nn}^k \boldsymbol{D}_{np} \boldsymbol{F}_S \boldsymbol{u}_S{}^k + \boldsymbol{C}_{nn}^k \boldsymbol{F}_{S,z} \boldsymbol{u}_S{}^k\right]$$
$$+ \left(\boldsymbol{F}_{\tau,z} \delta \boldsymbol{u}^k\right)^T \left[\boldsymbol{C}_{np}^k \boldsymbol{D}_p \boldsymbol{F}_S \boldsymbol{u}_S{}^k + \boldsymbol{C}_{nn}^k \boldsymbol{D}_{np} \boldsymbol{F}_S \boldsymbol{u}_S{}^k + \boldsymbol{C}_{nn}^k \boldsymbol{F}_{S,z} \boldsymbol{u}_S{}^k\right] \Big\} d\Omega_k dz \tag{18}$$
$$= \sum_{k=1}^{N_l} \int_{\Omega_k} \int_{A_k} \delta \boldsymbol{u}^k \boldsymbol{\rho} \ddot{\boldsymbol{u}}^k \, d\Omega_k dz$$

where the subscript z indicates the partial derivative with respect to z. Through the thickness, the integration of Eq. (18) yields:

$$\left(\boldsymbol{E}_{\tau spp}^k, \boldsymbol{E}_{\tau spn}^k, \boldsymbol{E}_{\tau s,zpn}^k\right) = \int_{A_k} \left(F_{m,\tau} F_{m,s} \boldsymbol{C}_{pp}^k, F_{m,\tau} F_{n,s} \boldsymbol{C}_{pn}^k, F_{m,\tau} \boldsymbol{C}_{pn}^k \boldsymbol{F}_{s,z}\right) dz \tag{19}$$

$$\left(\boldsymbol{E}^k_{\tau snp}, \boldsymbol{E}^k_{\tau snn}, \boldsymbol{E}^k_{\tau s_{,z} nn}\right) = \int_{A_k} \left(F_{n,\tau} F_{m,s} \boldsymbol{C}^k_{np}, F_{n,\tau} F_{n,s} \boldsymbol{C}^k_{nn}, F_{n,\tau} \boldsymbol{C}^k_{nn} \boldsymbol{F}_{\boldsymbol{s}_{,z}} \right) dz$$

$$\left(\boldsymbol{E}^k_{\tau_{,z} snp}, \boldsymbol{E}^k_{\tau_{,z} snn}, \boldsymbol{E}^k_{\tau_{,z} s_{,z} nn}\right) = \int_{A_k} \left(\boldsymbol{F}_{\boldsymbol{\tau}_{,z}} F_{m,s} \boldsymbol{C}^k_{np}, \boldsymbol{F}_{\boldsymbol{\tau}_{,z}} F_{n,s} \boldsymbol{C}^k_{nn}, \boldsymbol{F}_{\boldsymbol{\tau}_{,z}} \boldsymbol{C}^k_{nn} \boldsymbol{F}_{\boldsymbol{s}_{,z}} \right) dz$$

Now, by performing the integration of parts and using the following expression,

$$\int_{\Omega_k} (\boldsymbol{D}_\Omega \delta \boldsymbol{a}_\tau{}^k)^T \boldsymbol{a}_S{}^k d\Omega_k = - \int_{\Omega_k} \delta \boldsymbol{a}_\tau{}^{k^T} (\boldsymbol{D}_\Omega \boldsymbol{a}_S{}^k) d\Omega_k + \int_{\Gamma_k} \delta \boldsymbol{a}_\tau{}^{k^T} (\boldsymbol{I}_\Omega \boldsymbol{a}_S{}^k) d\Omega_k \tag{20}$$

and Eq. (15) is rewritten as follows:

$$\int_{\Omega_k} \{(\delta \boldsymbol{u}^k_\tau)^T \boldsymbol{K}^{k\tau s}_{uu} \boldsymbol{u}^k_s\} \, d\Omega_k + \int_{\Gamma_k} \{(\delta \boldsymbol{u}^k_\tau)^T \boldsymbol{\Pi}^{k\tau s}_{uu} \boldsymbol{u}^k_s\} \, d\Gamma_k = \sum_{k=1}^{N_l} \int_{\Omega_k} \int_{A_k} \delta \boldsymbol{u}^k \boldsymbol{\rho} \ddot{\boldsymbol{u}}^k \, d\Omega_k dz \tag{21}$$

where

$$\begin{aligned} \boldsymbol{K}^{k\tau s}_{uu} = &-\left(\boldsymbol{D}_p\right)^T \left[\boldsymbol{E}^k_{\tau spp} \boldsymbol{D}_p + \boldsymbol{E}^k_{\tau spn} \boldsymbol{D}_{np} + \boldsymbol{E}^k_{\tau s_{,z} pn}\right] - \left(\boldsymbol{D}_{np}\right)^T \left[\boldsymbol{E}^k_{\tau snp} \boldsymbol{D}_p + \boldsymbol{E}^k_{\tau snn} \boldsymbol{D}_{np} + \boldsymbol{E}^k_{\tau s_{,z} nn}\right] \\ &+ \left[\boldsymbol{E}^k_{\tau_{,z} snp} \boldsymbol{D}_p + \boldsymbol{E}^k_{\tau_{,z} snn} \boldsymbol{D}_{np} + \boldsymbol{E}^k_{\tau_{,z} s_{,z} nn}\right] \end{aligned} \tag{22}$$

Finally, the following compact differential equations can be achieved:

$$(\delta \boldsymbol{u}^k_\tau)^T: \qquad \boldsymbol{K}^{k\tau s}_{uu} \boldsymbol{u}^k_s = \boldsymbol{M}^{k\tau s}_{uu} \ddot{\boldsymbol{u}}^k_s \tag{23}$$

3. Naviers' Solution

Assuming that the FG plate is simply supported (see Refs. [27, 28] to consider other boundary conditions), the Navier closed form solution is chosen as a solution as follows:

$$\begin{aligned} u_x{}^K &= \sum\nolimits_{r,s} e^{i\omega t} U_x{}^K \cos(\alpha x) \sin(\beta y) \\ u_y{}^K &= \sum\nolimits_{r,s} e^{i\omega t} U_y{}^K \sin(\alpha x) \sin(\beta y) \\ u_z{}^K &= \sum\nolimits_{r,s} e^{i\omega t} U_z{}^K \sin(\alpha x) \sin(\beta y) \end{aligned} \tag{24a-c}$$

where $\alpha = r\pi/a$ and $\beta = s\pi/\mathrm{b}$. $U^k_{x_s}, U^k_{y_s}, U^k_{z_s}$ are amplitudes, and r and s are the number of semi-waves.

$$\begin{bmatrix} \bar{K}_{uu11} & \bar{K}_{uu12} & \bar{K}_{uu13} \\ \bar{K}_{uu21} & \bar{K}_{uu22} & \bar{K}_{uu23} \\ \bar{K}_{uu31} & \bar{K}_{uu32} & \bar{K}_{uu33} \end{bmatrix} \begin{bmatrix} U^k_{x_s} \\ U^k_{y_s} \\ U^k_{z_s} \end{bmatrix} = \begin{bmatrix} \bar{M}_{uu11} & 0 & 0 \\ 0 & \bar{M}_{uu22} & 0 \\ 0 & 0 & \bar{M}_{uu33} \end{bmatrix} \begin{bmatrix} \ddot{U}^k_{x_s} \\ \ddot{U}^k_{y_s} \\ \ddot{U}^k_{z_s} \end{bmatrix} \tag{25}$$

where

$$\bar{K}_{uu11} = \int_z \left(C_{55}(z) F_{m,\tau_{,z}} F_{m,s_{,z}} + \alpha^2 C_{11}(z) F_{m,\tau} F_{m,s} + \beta^2 C_{66}(z) F_{m,\tau} F_{m,s} \right) dz$$

$$\bar{K}_{uu12} = \int_z \left(\alpha\beta C_{12}(z) F_{m,\tau} F_{m,s} + \alpha\beta C_{66}(z) F_{m,\tau} F_{m,s} \right) dz$$

$$\bar{K}_{uu13} = \int_z \left(-\alpha C_{13}(z) F_{m,\tau} F_{n,s_{,z}} + \alpha C_{55}(z) F_{m,\tau_{,z}} F_{n,s} \right) dz \tag{26a-i}$$

$$\bar{K}_{uu21} = \int_z \left(\alpha\beta C_{12}(z) F_{m,\tau} F_{m,s} + \alpha\beta C_{66}(z) F_{m,\tau} F_{m,s} \right) dz$$

$$\bar{K}_{uu22} = \int_z \left(C_{44}(z) F_{m,\tau_{,z}} F_{m,s_{,z}} + \beta^2 C_{22}(z) F_{m,\tau} F_{m,s} + \alpha^2 C_{66}(z) F_{m,\tau} F_{m,s} \right) dz$$

$$\bar{K}_{uu23} = \int_z \left(-\beta C_{23}(z) F_{m,\tau} F_{n,s_{,z}} + \beta C_{44}(z) F_{m,\tau_{,z}} F_{n,s}\right) dz$$

$$\bar{K}_{uu31} = \int_z \left(\alpha C_{55}(z) F_{n,\tau} F_{m,s_{,z}} - \alpha C_{13}(z) F_{n,\tau_{,z}} F_{m,s}\right) dz$$

$$\bar{K}_{uu32} = \int_z \left(\beta C_{44}(z) F_{n,\tau} F_{m,s_{,z}} - \beta C_{23}(z) F_{n,\tau_{,z}} F_{m,s}\right) dz$$

$$\bar{K}_{uu33} = \int_z \left(C_{33}(z) F_{n,\tau_{,z}} F_{n,s_{,z}} + \beta^2 C_{44}(z) F_{m,\tau} F_{m,s} + \alpha^2 C_{55}(z) F_{m,\tau} F_{m,s}\right) dz$$

Finally

$$\bar{M}_{uu11} = \int_z \left(\rho(z) F_{m,\tau} F_{m,s}\right) dz$$

$$\bar{M}_{uu22} = \int_z \left(\rho(z) F_{m,\tau} F_{m,s}\right) dz \qquad (27a\text{-}c)$$

$$\bar{M}_{uu33} = \int_z \left(\rho(z) F_{n,\tau} F_{n,s}\right) dz$$

4. Results and discussions

Two issues related to the behavior of FG plates are addressed in the present study. Firstly, a static analysis of a simply supported FG square plate is performed using the CUF framework and employing a set of non-polynomial displacement fields to predict accurately the plate's displacements and stresses when the plate is subjected to the bi-sinusoidal pressure load (q_0), normal to the top face. The proposed displacement fields are given in Table 2.

$$q_0 = Q_0 \sin(\alpha x) \sin(\beta y) \qquad (28)$$

where $Q_0 = 1$. The results are presented in terms of the following non-dimensional parameters:

$$\bar{u} = u_x\left(0, \frac{b}{2}, -\frac{h}{4}\right)\frac{100h^3 E_c}{Q_0 a^4}, \qquad \bar{v} = u_x\left(\frac{a}{2}, 0, -\frac{h}{6}\right)\frac{10h^3 E_c}{Q_0 a^4},$$

$$\bar{w} = u_z\left(\frac{a}{2}, \frac{b}{2}, 0\right)\frac{10h^3 E_c}{Q_0 a^4}, \qquad \bar{\sigma}_{yy} = \sigma_{yy}\left(\frac{a}{2}, \frac{b}{2}, \frac{h}{3}\right)\frac{h}{Q_0 a} \qquad (29a\text{-}f)$$

$$\bar{\sigma}_{xy} = \sigma_{xy}\left(0, 0, -\frac{h}{3}\right)\frac{h}{Q_0 a}, \qquad \bar{\sigma}_{yz} = \sigma_{yz}\left(\frac{a}{2}, 0, \frac{h}{6}\right)\frac{h}{Q_0 a}$$

Table 2. SSSFs proposed in this paper.

Field	i	$F_{i,0}$	$F_{i,1}$	$F_{i,2}$	$F_{i,3}$	$F_{i,4}$
Polynomial	--	1	z	z^2	z^3	z^4
F1	m	1	z	$\sin(mz/h)$	$\cos(mz/h)$	$\sin(2mz/h)$
	n	1	z	$z.\sin(nz/h)$	$z.\cos(nz/h)$	$z.\sin(2\,nz/h)$
F2	m	1	z	$\cos(mz/h)$	$\sin(mz/h)$	$\cos(2\,mz/h)$
	n	1	z	$\sin(nz/h)$	$\cos(nz/h)$	$\sin(2\,nz/h)$
F3	m	1	z	$\tanh(mz/h)$	$\mathrm{sech}(mz/h)$	$\tanh(2\,mz/h)$
	n	1	z	$\cosh(nz/h)$	$\sinh(nz/h)$	$\cosh(2nz/h)$

Secondly, a free vibration analysis of a FG square plate (Al/ZrO_2) is performed employing an expansion order N=3 for the displacement fields. The results are given in terms of the following dimensionless frequencies:

$$\omega_{r,s}{}^{(k)} = \omega_{r,s}\frac{a^2}{h}\sqrt{\frac{\rho_m}{E_m}} \qquad (30)$$

where *r* and *s* are the wave numbers. In addition, the subscripts "*m*" and "*c*" denote metallic and ceramic, respectively. Finally, to ensure the validity of the presented outcomes, they are compared with the exact solutions found in the literature.

4.1. Static results

A FG square plate with the thickness, *h,* and the side-to-thickness ratio, $\frac{a}{h} = 10$, is considered. The plate is graded from aluminium at the bottom to alumina at the top. The Young's modulus and density are estimated by the law-of-mixtures (See Eq. 2). Figure 2 shows the ceramic volume fraction for different values of the exponent *p*.

As shown in Table 2, the displacement fields proposed in the current research use non-polynomial SSSF, more specifically, trigonometric and hyperbolic functions. Moreover, the SSSF are defined in terms of "*m*" and "*n*" parameters that could be varied. Therefore, the first analysis is performed using an expansion order, N=4, by assuming the arguments equal to one *(m=n=1)*. Table 3 presents the obtained results of displacements and stresses of the simply supported FG square plate for a set of values of $p = \{1, 2, 3, 5\}$. It can be noticed that the results are in a good agreement with 2D analytical solution by Carrera et al. [20]. Then, a second analysis is performed using the expansion order, N=2. The obtained outcomes are compared with respect to the referential solution to check accuracy. Fortunately, it is possible to improve accuracy with a fixed number of variables, i.e., fixed N, as shown in Ref. [26]. To this end, it is necessary to develop a process of optimization in which the arguments (*m*, *n*) are varied to find the best match with 3D elasticity solution or referential solution. The Optimization 1 (Opt. 1) model is defined to get a couple of *m* and *n* parameters that allows obtaining good results (minimum error) for displacements. Other optimization models are also explored and they are presented as follows:

$$Optimization\ 1\ for\ \min[\frac{\%Err_u + \%Err_v + \%Err_w}{3}]$$
$$Optimization\ 2\ for\ \min[\frac{\%Err_{\sigma_{yy}} + \%Err_{\sigma_{yz}} + \%Err_{\sigma_{xy}}}{3}] \quad (31a\text{-}c)$$
$$Optimization\ 3\ for\ \min[\frac{\%Err_u + \%Err_v + \%Err_w + \%Err_{\sigma_{yy}} + \%Err_{\sigma_{yz}} + \%Err_{\sigma_{xy}}}{6}]$$

where

$$\%Err_u = \frac{u_{present} - u_{exact}}{u_{exact}} \times 100\% \quad (32)$$

Equation 32 allows obtaining the accuracy of the results by comparing the obtained results and the exact solution or the referential solution.

Figures 3 to 5 illustrate the correspondence between the arguments (*m*, *n*) with the accuracy of the outcomes for *p*=5. For example, Fig. 3 shows three graphics, each one corresponds to an optimization process (mentioned in Eq. 31). Furthermore, the case of study is solved using the proposed first displacement field (see Table 1). Analyzing results reported in Fig. 3, it is possible to observe the variation of errors (obtained in Eq. 32) as a function of "m" and "n" parameters. Therefore, at one glance, the first graph (Optimization 1) shows that the region with low level of error is in the neighborhood of the point (1, 1); whereas, for Optimization 2 and 3, good results are found in the neighborhood of the point (0, 0). The same analysis is presented in Figs. 4 and 5.

In addition, the optimum values of the arguments are presented in Table 4. Then, using these optimum values, the FG plate's displacements and stresses are calculated and presented in Table 5. Again, the obtained outcomes are compared with 2D analytical solutions given by Carrera [20].

Table 3. Comparison of non-dimensional 2D analytical solution of displacements and stress of a FG square plate (Al/Al_2O_3) ($N = 4, a = b, a/h = 10, m = 1 \,\&\, n = 1$).

p	*Theory*	$\bar{u}$	$\bar{v}$	$\bar{w}$	$\bar{\sigma}_{yy}$	$\bar{\sigma}_{yz}$	$\bar{\sigma}_{xy}$
	Nml = 100(PVD) [20]	***0.6436***	***0.4970***	***0.5875***	***1.5062***	***0.2510***	***0.6081***
	Polynomial (N=4)	0.6435	0.4981	0.5875	1.5064	0.2508	0.6112
1	*F1 (N=4)*	0.6429	0.4976	0.5865	1.3965	0.2523	0.6105
	F2 (N=4)	0.6437	0.4981	0.5875	1.5057	0.2546	0.6114
	F3 (N=4)	0.6437	0.4981	0.5875	1.5059	0.2539	0.6114
	Nml = 100(PVD) [20]	***0.9012***	***0.7149***	***0.7570***	***1.4147***	***0.2496***	***0.5421***
	Polynomial (N=4)	0.9012	0.7162	0.7570	1.4140	0.2514	0.5437
2	*F1 (N=4)*	0.9009	0.7154	0.7554	1.2864	0.2615	0.5437
	F2 (N=4)	0.9021	0.7161	0.7568	1.4119	0.2641	0.5445
	F3 (N=4)	0.9020	0.7161	0.7569	1.4124	0.2622	0.5444
	Nml = 100(PVD) [20]	***1.0106***	***0.8065***	***0.8381***	***1.2948***	***0.2420***	***0.5515***
	Polynomial (N=4)	1.0111	0.8086	0.8381	1.2936	0.2447	0.5522
3	*F1 (N=4)*	1.0106	0.8069	0.8361	1.1599	0.2600	0.5525
	F2 (N=4)	1.0119	0.8076	0.8377	1.2911	0.2626	0.5534
	F3 (N=4)	1.0119	0.8077	0.8378	1.2918	0.2599	0.5533
	Nml = 100(PVD) [20]	***1.0716***	***0.8506***	***0.9118***	***1.1233***	***0.2324***	***0.5761***
	Polynomial (N=4)	1.0724	0.8540	0.9116	1.1219	0.2270	0.5763
5	*F1 (N=4)*	1.0707	0.8511	0.9099	0.9899	0.2390	0.5762
	F2 (N=4)	1.0719	0.8518	0.9117	1.1201	0.2414	0.5771
	F3 (N=4)	1.0719	0.8517	0.9117	1.1208	0.2390	0.5770

Table 4. Optimum values of arguments (m, n) of the non-polynomial SSSFs for the bending analysis ($N = 2$).

	F1 (N=2)		*F2 (N=2)*		*F3 (N=2)*	
p=1	m	n	m	n	m	n
Optimization 1st	1	0.8	0.1	0.1	0.1	0.3
Optimization 2nd	7.4	0.1	7	0.1	3.9	0.7
Optimization 3rd	0.1	0.1	7	0.1	3.9	0.7
p=2	m	n	m	n	m	n
Optimization 1st	0.2	0.1	0.1	0.1	0.1	0.4
Optimization 2nd	0.1	0.6	7	0.1	5	0.9
Optimization 3rd	0.1	0.1	7	0.1	5	0.9
p=3	m	n	m	n	m	n
Optimization 1st	0.7	0.3	0.1	0.1	0.1	0.5
Optimization 2nd	0.1	0.3	7	0.1	5.3	1
Optimization 3rd	0.1	0.1	7	0.1	5.3	1
p=5	m	n	m	n	m	n
Optimization 1st	0.3	0.2	0.2	0.1	0.1	0.7
Optimization 2nd	0.1	0.2	7	0.1	4.3	1.4
Optimization 3rd	0.1	0.1	7	0.1	4.3	1.4

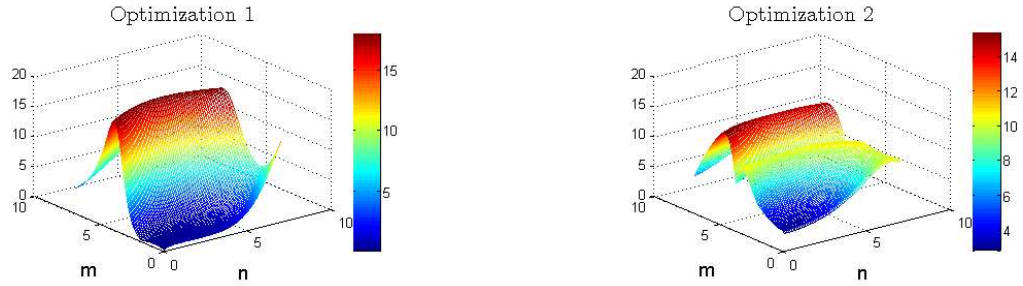

Fig. 3. Error (%) obtained from optimization procedures on the first SSSFs (Al/Al_2O_3, $a = b, a/h = 10$ & $p = 5$).

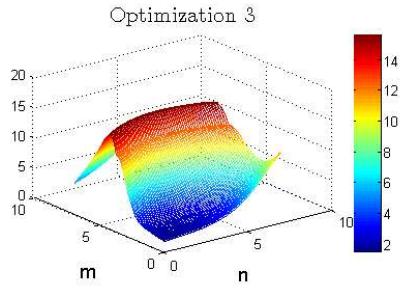

Fig. 3. (continued)

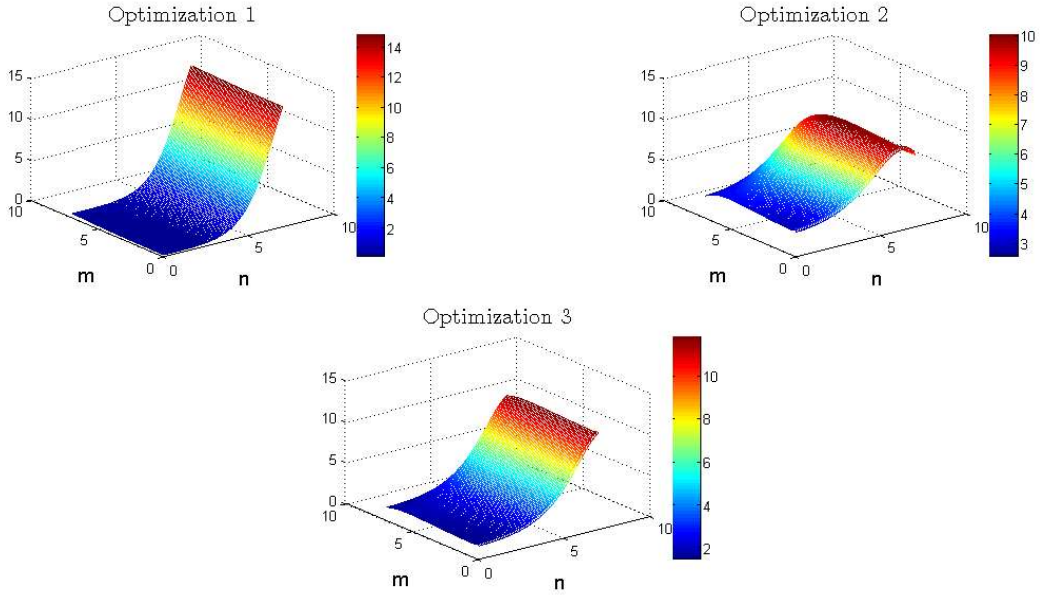

Fig. 4. Error (%) obtained from optimization procedures on the second SSSFs (Al/Al_2O_3, $a = b, a/h = 10$ & $p = 5$).

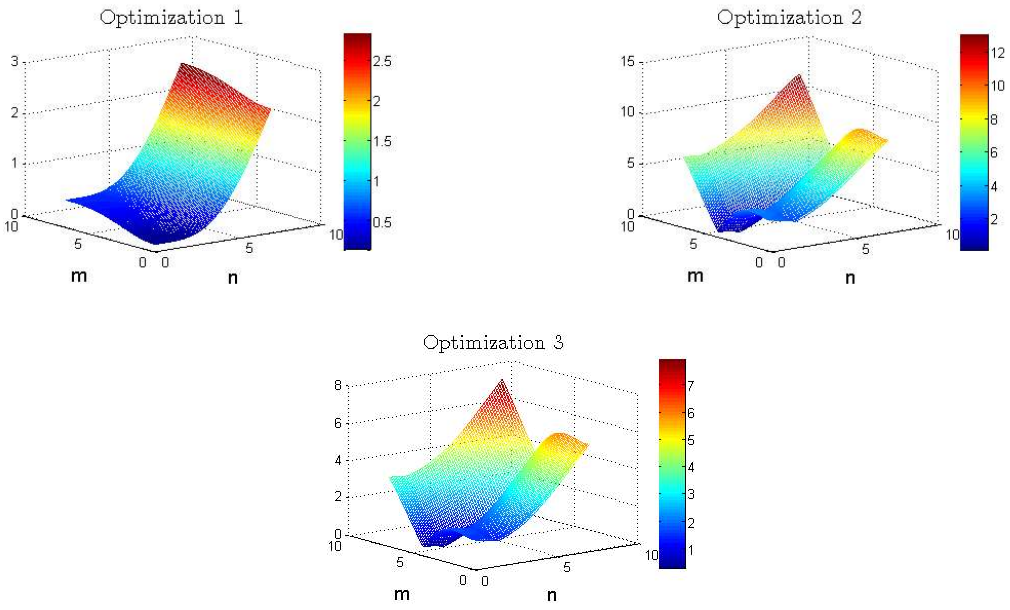

Fig. 5. Error (%) obtained from optimization procedures on the third SSSFs (Al/Al_2O_3, $a = b, a/h = 10$ & $p = 5$).

Table 5. Comparison of non-dimensional displacements and stress of a FG square plate (Al/Al_2O_3) ($N = 2, a = b, a/h = 10$).

p	*Theory*	$\bar{u}$	$\bar{v}$	$\bar{w}$	$\bar{\sigma}_{yy}$	$\bar{\sigma}_{yz}$	$\bar{\sigma}_{xy}$
	N_{ml} = 100(PVD) [20]	**0.6436**	**0.4970**	**0.5875**	**1.5062**	**0.2510**	**0.6081**
	Polynomial (N=2)	0.6463	0.5012	0.5853	1.5099	0.1997	0.6121
	F1 (N=2) Opt 1st	0.6436	0.4971	0.5875	1.4905	0.2672	0.6123
	F1 (N=2) Opt 2nd	0.6117	0.4716	0.5592	1.5065	0.2552	0.5833
1	*F1 (N=2) Opt 3rd*	0.6432	0.4969	0.5872	1.5010	0.2674	0.6119
	F2 (N=2) Opt 1st	0.6432	0.4969	0.5872	1.5011	0.2674	0.6119
	F2 (N=2) Opt 2nd	0.6428	0.4960	0.5867	1.5028	0.2581	0.6122
	F3 (N=2) Opt 1st	0.6432	0.4969	0.5872	1.5016	0.2674	0.6119
	F3 (N=2) Opt 2nd	0.6429	0.4959	0.5867	1.5060	0.2510	0.6124
	N_{ml} = 100(PVD) [20]	**0.9012**	**0.7149**	**0.7570**	**1.4147**	**0.2496**	**0.5421**
	Polynomial (N=2)	0.9066	0.7213	0.7533	1.4166	0.2001	0.5454
	F1 (N=2) Opt 1st	0.9030	0.7149	0.7570	1.4021	0.2824	0.5465
	F1 (N=2) Opt 2nd	0.8960	0.7095	0.7524	1.4093	0.2822	0.5421
2	*F1 (N=2) Opt 3rd*	0.9007	0.7132	0.7555	1.4053	0.2824	0.5451
	F2 (N=2) Opt 1st	0.9007	0.7132	0.7555	1.4053	0.2824	0.5451
	F2 (N=2) Opt 2nd	0.8997	0.7114	0.7549	1.4069	0.2742	0.5452
	F3 (N=2) Opt 1st	0.9007	0.7132	0.7555	1.4064	0.2824	0.5451
	F3 (N=2) Opt 2nd	0.9002	0.7111	0.7543	1.4148	0.2499	0.5456
	N_{ml} = 100(PVD) [20]	**1.0106**	**0.8065**	**0.8381**	**1.2948**	**0.2420**	**0.5515**
	Polynomial (N=2)	1.0192	0.8158	0.8316	1.2961	0.1852	0.5549
	F1 (N=2) Opt 1st	1.0130	0.8064	0.8376	1.2729	0.2781	0.5553
	F1 (N=2) Opt 2nd	1.0064	0.8013	0.8335	1.2865	0.2779	0.5515
3	*F1 (N=2) Opt 3rd*	1.0101	0.8042	0.8359	1.2830	0.2780	0.5537
	F2 (N=2) Opt 1st	1.0101	0.8042	0.8359	1.2831	0.2780	0.5537
	F2 (N=2) Opt 2nd	1.0083	0.8014	0.8353	1.2840	0.2730	0.5538
	F3 (N=2) Opt 1st	1.0101	0.8042	0.8359	1.2848	0.2781	0.5537
	F3 (N=2) Opt 2nd	1.0090	0.8007	0.8342	1.2879	0.2412	0.5543
	N_{ml} = 100(PVD) [20]	***1.0716***	***0.8506***	***0.9118***	***1.1233***	***0.2324***	***0.5761***
	Polynomial (N=2)	1.0833	0.8643	0.9001	1.1244	0.1529	0.5796
	F1 (N=2) Opt 1st	1.0723	0.8505	0.9112	1.1068	0.2500	0.5780
	F1 (N=2) Opt 2nd	1.0682	0.8473	0.9085	1.1115	0.2494	0.5757
5	*F1 (N=2) Opt 3rd*	1.0708	0.8494	0.9102	1.1093	0.2494	0.5772
	F2 (N=2) Opt 1st	1.0705	0.8492	0.9106	1.1089	0.2520	0.5771
	F2 (N=2) Opt 2nd	1.0678	0.8451	0.9096	1.1090	0.2470	0.5772
	F3 (N=2) Opt 1st	1.0708	0.8494	0.9102	1.1125	0.2495	0.5772
	F3 (N=2) Opt 2nd	1.0681	0.8443	0.9092	1.1234	0.2327	0.5775

4.2. Free vibration results

The first nine thickness mode frequencies corresponding to wave numbers *r=s=1* is studied in this section. A FG square plate with the thickness, *h,* and the side-to-thickness ratio, $a/h = 5$, is selected. The plate is graded from aluminum (bottom) to zirconia (top), and the Mori-Tanaka method is used to calculate the effective properties of the FG plate. Figure 6 depicts the volume fraction, Poisson's ratio, Young's modulus, and density of the plate estimated by the Mori-Tanaka approach.

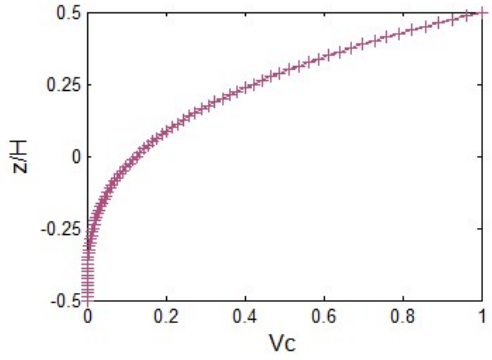

(a)

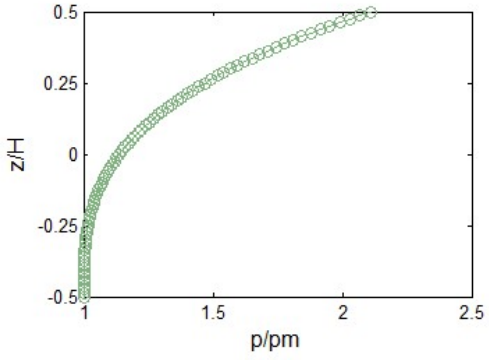

(b)

Fig. 6. Through the thickness distribution of (a) ceramic volume faction, (b) density, (c) Young's modulus and (d) Poisson ratio ($a/h = 5$ & $p = 3$).

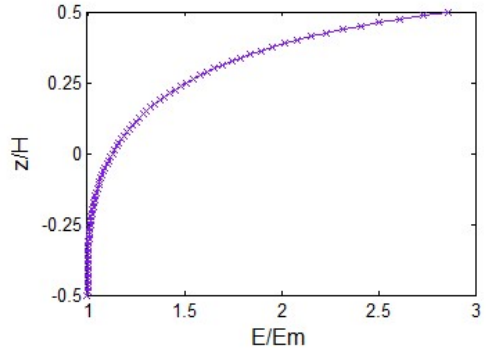

(c)

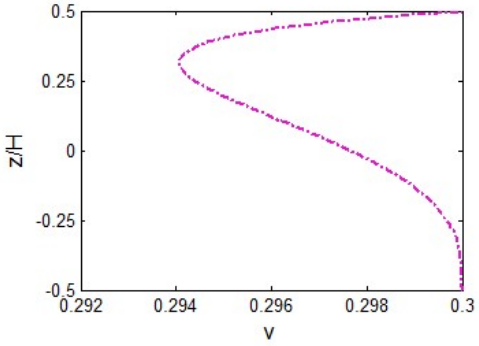

(d)

Fig. 6. (continued)

A free vibration analysis is performed for the expansion N=3 along with the arguments given by the following optimization model:

$$Optimization\ 4\ for\ \min[\%Err_{\omega 1} = \frac{{\omega^1}_{present} - {\omega^1}_{exact}}{{\omega^1}_{exact}} \times 100\%] \tag{33}$$

Therefore, the optimum values of the arguments are given in Table 6 for the expansion N=3. In addition, Fig. 7 shows three graphics, each one corresponds to a displacement field presented in Table 1, and likewise Fig. 3, it shows the accuracy of the results using the error given in Eq. 33.

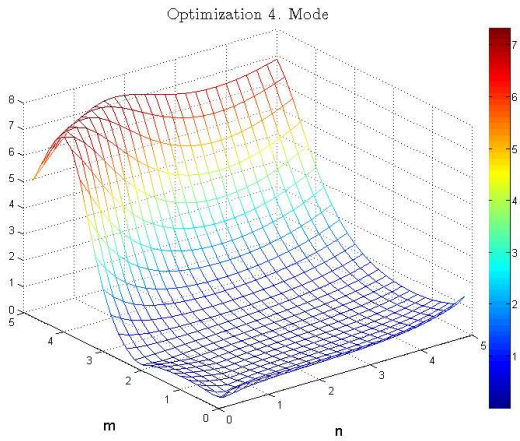

(a)

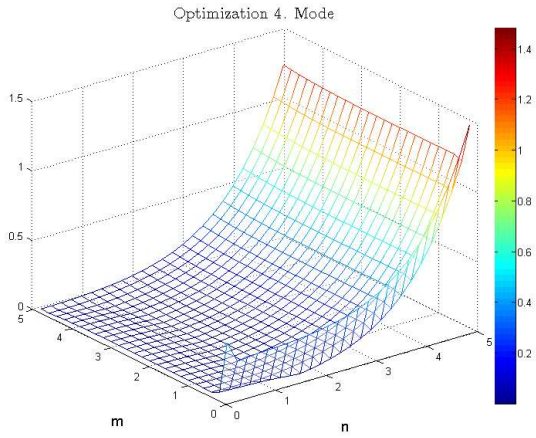

(b)

Fig. 7. Variations of dimensionless first thickness frequency (Opt. 4) with parameters "*m*" and "*n*". (a) First displacement field, (b) Second displacement field, (c) Third displacement field ($N = 3, a/h = 5$ & $p = 3$).

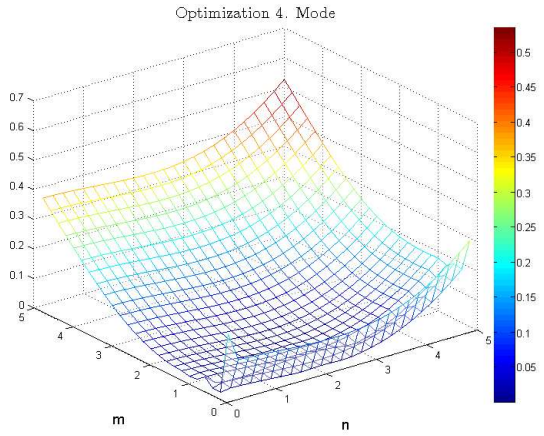

(c)

Fig. 7. (continued)

Table 6. Optimum values of arguments (m, n) of the non-polynomial displacement fields proposed for the vibration analysis ($N = 3$).

	F1 (N=3)		*F2 (N=3)*		*F3 (N=3)*	
Optimization 4th	m	n	m	n	m	n
p=1	1.3	1.3	0.3	1.9	0.7	0.9
p=2	2.1	0.5	0.7	1.3	0.3	1.1
p=3	0.7	0.7	4.1	1.1	0.9	2.5
p=5	1.9	0.9	0.9	0.5	0.7	0.5
Optimization 5th	m	n	m	n	m	n
p=1	5.7	3.7	5.7	5.1	2.1	4.1
p=2	5.7	3.7	5.7	5.1	2.3	3.1
p=3	5.7	3.7	5.9	5.1	2.3	0.5
p=5	5.5	3.9	5.7	4.5	2.5	5.5

Moreover, Table 7 presents the comparison between the obtained results using values presented in Table 6 and the exact solution presented by Vel [6]. Additionally, this table exhibits the frequencies obtained by a polynomial displacement field for the expansion N=50. Evidently, the outcomes obtained for an expansion N=3 are in an excellent agreement with Vel's outcomes for the first five thickness mode frequencies. However, the situation is completely different for the remaining frequencies. In order to overcome this inconvenient, an Optimization 5 (Opt. 5) model is used.

$$Optimization\ 5\ for\ \min[\%Err_{\omega 6} = \frac{{\omega^6}_{present} - {\omega^6}_{exact}}{{\omega^6}_{exact}} \times 100\%] \tag{34}$$

Table 7. Comparison of non-dimensional natural thickness frequencies for a FG (Al/ZrO_2) square plate ($N = 3, a = b, a/h = 5$), Opt.4.

Theory	${\omega_{1,1}}^{(1)}$	${\omega_{1,1}}^{(2)}$	${\omega_{1,1}}^{(3)}$	${\omega_{1,1}}^{(4)}$	${\omega_{1,1}}^{(5)}$	${\omega_{1,1}}^{(6)}$	${\omega_{1,1}}^{(7)}$	${\omega_{1,1}}^{(8)}$	${\omega_{1,1}}^{(9)}$
$a/h = 5\ \ p = 1$									
Vel [6]	**5.4806**	**14.558**	**24.381**	**53.366**	**57.620**	**90.993**	**102.97**	**109.37**	**152.63**
Poly (N=5)	5.4772	14.549	24.366	53.330	57.581	91.015	103.47	109.81	151.19
Poly (N=4)	5.4772	14.549	24.366	53.349	57.609	91.289	104.34	110.61	188.78
F1* (N=3)	5.4806	14.588	24.366	53.506	57.823	93.589	123.90	127.69	216.29
F2* (N=3)	5.4806	14.549	24.366	53.521	57.826	93.685	125.27	129.35	217.97
F3* (N=3)	5.4806	14.549	24.369	53.629	57.975	93.487	116.39	121.10	217.53
$a/h = 5\ \ p = 2$									
Vel [6]	**5.4923**	**14.278**	**23.909**	**50.376**	**54.685**	**86.190**	**99.921**	**105.66**	**148.97**
Poly (N=5)	5.4897	14.271	23.898	50.345	54.652	86.235	100.76	106.45	151.04
Poly (N=4)	5.4898	14.271	23.898	50.390	54.709	86.520	101.45	107.09	184.55
F1* (N=3)	5.4924	14.271	23.898	50.511	55.112	88.011	120.95	124.97	217.91
F2* (N=3)	5.4923	14.271	23.899	50.552	54.947	88.564	124.49	128.31	221.58
F3* (N=3)	5.4923	14.271	23.904	50.588	54.989	88.832	120.42	124.32	220.83
$a/h = 5\ \ p = 3$									
Vel [6]	**5.5285**	**14.150**	**23.696**	**48.825**	**53.179**	**83.700**	**98.730**	**104.17**	**147.53**
Poly (N=5)	5.5265	14.145	23.688	48.790	53.139	83.755	99.771	105.16	149.29
Poly (N=4)	5.5268	14.145	23.688	48.861	53.227	84.046	100.23	105.60	182.82
F1* (N=3)	5.5285	14.145	23.688	48.949	53.399	85.823	124.76	128.45	220.57
F2* (N=3)	5.5283	14.145	23.689	48.836	53.276	84.824	110.22	115.05	206.25
F3* (N=3)	5.5285	14.145	23.692	48.970	53.468	85.733	115.53	119.69	216.66

Table 7. (continued)

$a/h = 5\ \ p = 5$									
Vel [6]	**5.5632**	**14.026**	**23.494**	**47.687**	**52.068**	**81.825**	**97.384**	**102.71**	**146.02**
Poly (N=5)	5.5618	14.022	23.489	47.640	52.005	81.854	98.823	104.09	145.56
Poly (N=4)	5.5624	14.022	23.486	47.735	52.122	82.161	98.955	104.24	181.08
F1* (N=3)	5.5632	14.022	23.489	47.720	52.286	83.577	121.47	125.27	219.16
F2* (N=3)	5.5632	14.022	23.489	47.737	52.215	83.764	124.17	127.81	219.96
F3* (N=3)	5.5632	14.022	23.494	47.729	52.210	83.757	117.30	121.22	217.67

*Optimization 4th.

The optimum values of the arguments are presented in Table 6 for each displacement field and different values of p, which confirms the *case dependent problem* between the selected theory and the case study. As expected, the results of the sixth, seventh, and eighth frequencies are in a close agreement with the exact solution (Table 8).

The second free vibration analysis for the expansion N=2 is performed while the first five obtained frequencies are in a good agreement with the reference values (Table 9). However, for the expansion N=2, it is not possible to predict high frequencies even when the Optimization 5 is used. Consequently, other non-polynomial SSSFs should be evaluated or a zigzag variable expansion term should be included.

Table 8. Comparison of non-dimensional natural thickness frequencies for a FG (Al/ZrO_2) square plate ($N = 3, a = b, a/h = 5$), Opt. 4 and 5.

Theory	$\omega_{1,1}{}^{(1)}$	$\omega_{1,1}{}^{(2)}$	$\omega_{1,1}{}^{(3)}$	$\omega_{1,1}{}^{(4)}$	$\omega_{1,1}{}^{(5)}$	$\omega_{1,1}{}^{(6)}$	$\omega_{1,1}{}^{(7)}$	$\omega_{1,1}{}^{(8)}$	$\omega_{1,1}{}^{(9)}$
$a/h = 5\ \ p = 1$									
Vel [6]	**5.4806**	**14.558**	**24.381**	**53.366**	**57.620**	**90.993**	**102.97**	**109.37**	**152.63**
Poly (N=5)	5.4772	14.549	24.366	53.330	57.581	91.015	103.47	109.81	151.19
F1** (N=3)	5.4806	14.588	24.366	53.506	57.823	91.468	104.18	110.96	157.07
F2** (N=3)	5.4806	14.549	24.366	53.521	57.826	91.096	104.18	110.94	187.03
F3** (N=3)	5.4806	14.549	24.369	53.629	57.975	91.004	101.54	109.21	198.56
$a/h = 5\ \ p = 2$									
Vel [6]	**5.4923**	**14.278**	**23.909**	**50.376**	**54.685**	**86.190**	**99.921**	**105.66**	**148.97**
Poly (N=5)	5.4897	14.271	23.898	50.345	54.652	86.235	100.76	106.45	151.04
F1** (N=3)	5.4924	14.271	23.898	50.511	55.112	86.576	101.51	107.59	154.66
F2** (N=3)	5.4923	14.271	23.899	50.552	54.947	86.269	101.51	107.65	185.57
F3** (N=3)	5.4923	14.271	23.904	50.588	54.989	86.179	98.839	105.79	195.66
$a/h = 5\ \ p = 3$									
Vel [6]	**5.5285**	**14.150**	**23.696**	**48.825**	**53.179**	**83.700**	**98.730**	**104.17**	**147.53**
Poly (N=5)	5.5265	14.145	23.688	48.790	53.139	83.755	99.771	105.16	149.29
F1** (N=3)	5.5285	14.145	23.688	48.949	53.399	83.853	99.735	105.45	160.35
F2** (N=3)	5.5283	14.145	23.689	48.836	53.276	83.731	100.49	106.35	184.95
F3** (N=3)	5.5285	14.145	23.692	48.970	53.468	83.750	99.192	105.48	195.55
$a/h = 5\ \ p = 5$									
Vel [6]	**5.5632**	**14.026**	**23.494**	**47.687**	**52.068**	**81.825**	**97.384**	**102.71**	**146.02**
Poly (N=5)	5.5618	14.022	23.489	47.640	52.005	81.854	98.823	104.09	145.56
F1** (N=3)	5.5632	14.022	23.489	47.720	52.286	81.821	100.21	105.77	154.93
F2** (N=3)	5.5632	14.022	23.489	47.737	52.215	81.823	99.200	104.99	187.23
F3** (N=3)	5.5632	14.022	23.494	47.729	52.210	81.876	96.383	102.95	191.39

** Optimization 4th is used for the first six frequencies and Optimization 5th for the remain.

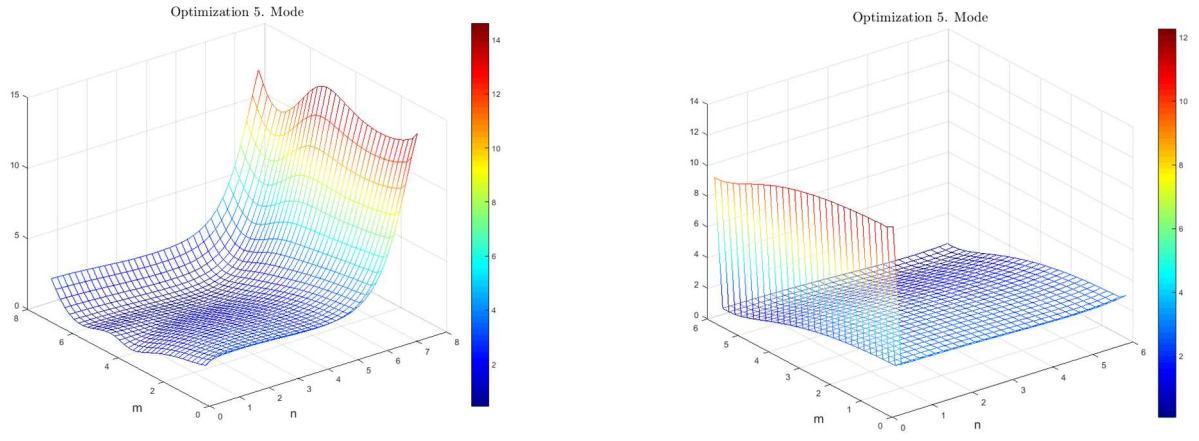

(a) (b)

Fig. 8. Variations of dimensionless sixth thickness frequency (Opt. 5) with parameters "m" and "n". (a) First displacement field, (b) Second displacement field, (c) Third displacement field ($N = 3, a/h = 5$ & $p = 2$).

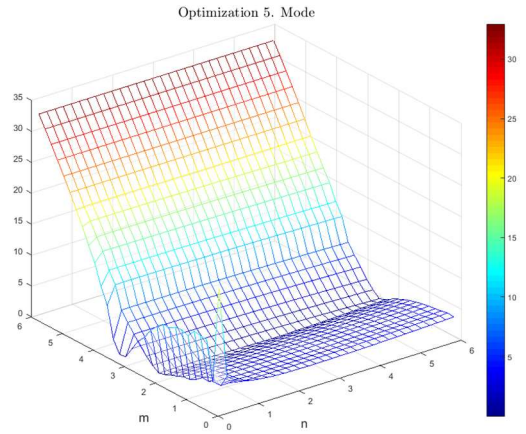

(c)

Fig. 8. (continued)

Table 9. Optimum values of arguments (m, n) of the non-polynomial SSSFs for the vibration analysis ($N = 2$).

	F1 (N=2)		*F2 (N=2)*		*F3 (N=2)*	
Optimization 4th	m	n	m	n	m	n
p=1	0.9	0.7	0.3	0.1	0.3	2.1
p=2	1.5	0.7	2.5	0.1	1.1	2.1
p=3	0.9	0.7	0.3	0.3	0.3	2.1
p=5	1.1	0.9	0.3	1.3	1.3	1.3
Optimization 5th	m	n	m	n	m	n
p=1	7.1	2.9	5.9	0.1	3.7	3.3
p=2	7.1	2.9	5.9	0.1	3.5	4.1
p=3	7.1	2.9	0.3	0.1	3.3	5.9
p=5	7.1	2.9	0.3	0.1	0.1	2.3

In addition to the presented results, the free vibration analysis of advanced composites with law-of-mixtures is performed to estimate the properties of the plate. The results are compared with 2D analytical solutions given by Matsunaga [12] (Table 10). Table 11 represents that flexural free vibration frequency results are in a good agreement when compared with respect to 3D exact solution. Finally, the obtained flexural modes are shown in Figs. 9 to 11, which are comparable with modes presented by Neves [19].

Overall, it is important to notice that the available benchmark examples in the literature use higher order expansion than those proposed in the present study. For instance, the exact solution for the vibration of FG plates presented by Vel [6] was obtained using fifty terms in the power series proposed as the displacement function, whereas Carrera [20] utilized an expansion order N=4 to develop the static analysis of functionally graded plates subjected to transverse mechanical loadings.

Table 10. Comparison of non-dimensional natural thickness frequencies for a FG (Al/ZrO_2) square plate ($N = 2, a = b, a/h = 5$) , Opt.4.

Theory	$\omega_{1,1}{}^{(1)}$	$\omega_{1,1}{}^{(2)}$	$\omega_{1,1}{}^{(3)}$	$\omega_{1,1}{}^{(4)}$	$\omega_{1,1}{}^{(5)}$	$\omega_{1,1}{}^{(6)}$	$\omega_{1,1}{}^{(7)}$	$\omega_{1,1}{}^{(8)}$	$\omega_{1,1}{}^{(9)}$
$a/h = 5\ \ p = 1$									
Vel [6]	**5.4806**	**14.558**	**24.381**	**53.366**	**57.620**	**90.993**	**102.97**	**109.37**	**152.63**
F1** (N=2)	5.4807	14.549	24.422	53.730	58.117	103.92	175.50	175.73	253.45
F2** (N=2)	5.4821	14.549	24.421	53.734	58.057	106.28	189.11	190.27	242.99
F3** (N=2)	5.4820	14.549	24.421	53.716	58.063	106.24	178.61	180.13	263.29
$a/h = 5\ \ p = 2$									
Vel [6]	**5.4923**	**14.278**	**23.909**	**50.376**	**54.685**	**86.190**	**99.921**	**105.66**	**148.97**
F1** (N=2)	5.4921	14.271	23.964	50.713	55.227	99.702	174.09	174.41	255.50
F2** (N=2)	5.4958	14.271	23.964	50.688	55.086	102.24	188.67	189.86	241.95
F3** (N=2)	5.4955	14.271	23.964	50.743	55.140	102.17	179.70	181.24	274.77
$a/h = 5\ \ p = 3$									
Vel [6]	**5.5285**	**14.150**	**23.696**	**48.825**	**53.179**	**83.700**	**98.730**	**104.17**	**147.53**
F1** (N=2)	5.5289	14.145	23.759	49.039	53.534	97.535	173.29	173.61	255.43
F2** (N=2)	5.5296	14.145	23.759	49.036	53.411	100.23	221.17	222.16	242.16
F3** (N=2)	5.5296	14.145	23.759	49.004	53.506	100.06	181.54	183.10	309.21
$a/h = 5\ \ p = 5$									
Vel [6]	**5.5632**	**14.026**	**23.494**	**47.687**	**52.068**	**81.825**	**97.384**	**102.71**	**146.02**
F1** (N=2)	5.5630	14.023	23.563	47.748	52.255	95.827	171.70	171.98	252.83
F2** (N=2)	5.5633	14.023	23.563	47.658	52.124	98.676	218.24	218.19	239.64
F3** (N=2)	5.5636	14.023	23.563	47.734	52.220	89.543	98.636	214.14	249.24

** Optimization 4th is used for the first six frequencies and Optimization 5th for the remain.

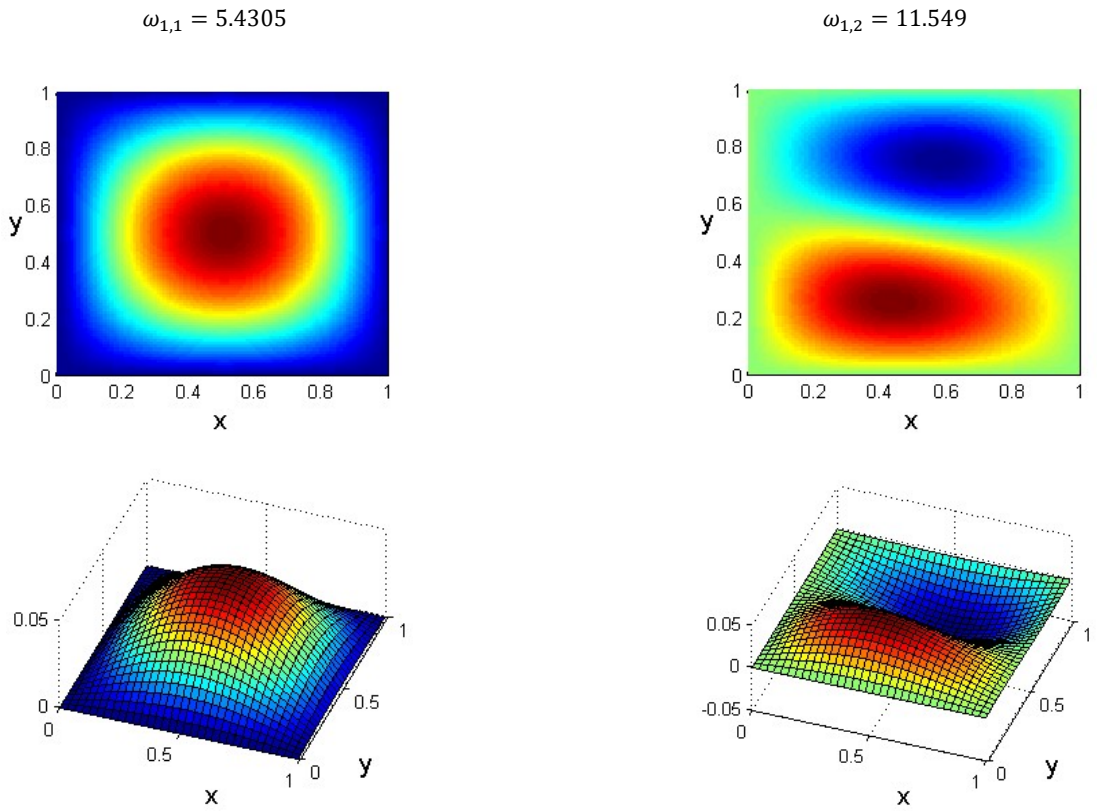

Fig. 9. Dimensionless flexural mode natural frequencies $\omega_{1,1}$ y $\omega_{1,2}$ of square FG plate (Al/ZrO₂) ($a = b, a/h = 5$ & $p = 1$).

Table 11. Comparison of non-dimensional natural thickness frequencies for a FG (Al/ZrO₂) square plate ($N = 2, a = b, a/h = 5$) , Opt. 4 and 5.

Theory	$\omega_{1,1}{}^{(1)}$	$\omega_{1,1}{}^{(2)}$	$\omega_{1,1}{}^{(3)}$	$\omega_{1,1}{}^{(4)}$	$\omega_{1,1}{}^{(5)}$	$\omega_{1,1}{}^{(6)}$	$\omega_{1,1}{}^{(7)}$	$\omega_{1,1}{}^{(8)}$	$\omega_{1,1}{}^{(9)}$
$a/h = 5\ \ p = 1$									
Matsunaga [12]	**5.7123**	**15.339**	**25.776**	**57.114**	**61.509**	**97.859**	**109.16**	**116.67**	**161.43**
Poly (N=5)	5.7123	15.341	25.776	57.108	61.503	97.937	109.63	117.08	161.64
F1* (N=2)	5.7142	15.341	25.821	57.457	61.989	113.11	225.10	225.94	281.89
F2* (N=2)	5.7163	15.341	25.821	57.459	61.941	113.22	225.75	225.85	252.86
F3* (N=2)	5.7157	15.341	25.821	57.456	61.974	113.19	225.16	225.70	260.46
$a/h = 5\ \ p = 2$									
Matsunaga [12]	**5.6599**	**14.970**	**25.140**	**53.188**	**57.576**	**91.483**	**104.82**	**111.22**	**155.99**
Poly (N=5)	5.6599	14.972	25.140	53.183	57.572	91.568	105.45	111.81	158.41
F1* (N=2)	5.6638	14.972	25.190	53.811	58.423	106.63	225.03	226.24	354.18
F2* (N=2)	5.6682	14.972	25.190	53.792	58.277	106.99	221.32	221.71	251.26
F3* (N=2)	5.6673	14.972	25.190	53.783	58.307	106.99	219.11	219.91	259.40
$a/h = 5\ \ p = 3$									
Matsunaga [12]	**5.6757**	**14.150**	**24.741**	**50.790**	**55.237**	**87.481**	**102.76**	**108.52**	**153.30**
Poly (N=5)	5.6757	14.743	24.741	50.782	55.229	87.561	103.60	109.32	155.95
F1* (N=2)	5.6817	14.743	24.802	51.324	55.922	103.64	227.34	228.19	279.68
F2* (N=2)	5.6839	14.743	24.802	51.329	55.880	103.75	228.02	228.07	251.17
F3* (N=2)	5.6828	14.743	24.802	51.324	55.914	103.74	227.44	228.01	259.64
$a/h = 5\ \ p = 5$									
Matsunaga [12]	**5.7020**	**14.026**	**24.278**	**48.772**	**53.288**	**83.914**	**100.24**	**105.63**	**150.24**
Poly (N=5)	5.7020	14.477	24.278	48.754	53.268	83.988	101.34	106.69	153.18
F1* (N=2)	5.7053	14.477	24.353	49.005	53.659	101.09	227.16	227.82	266.97
F2* (N=2)	5.7073	14.477	24.353	49.007	53.620	101.15	225.87	226.06	245.84
F3* (N=2)	5.7050	14.477	24.353	48.930	53.573	101.10	216.99	217.70	251.97

*Optimization 4th.

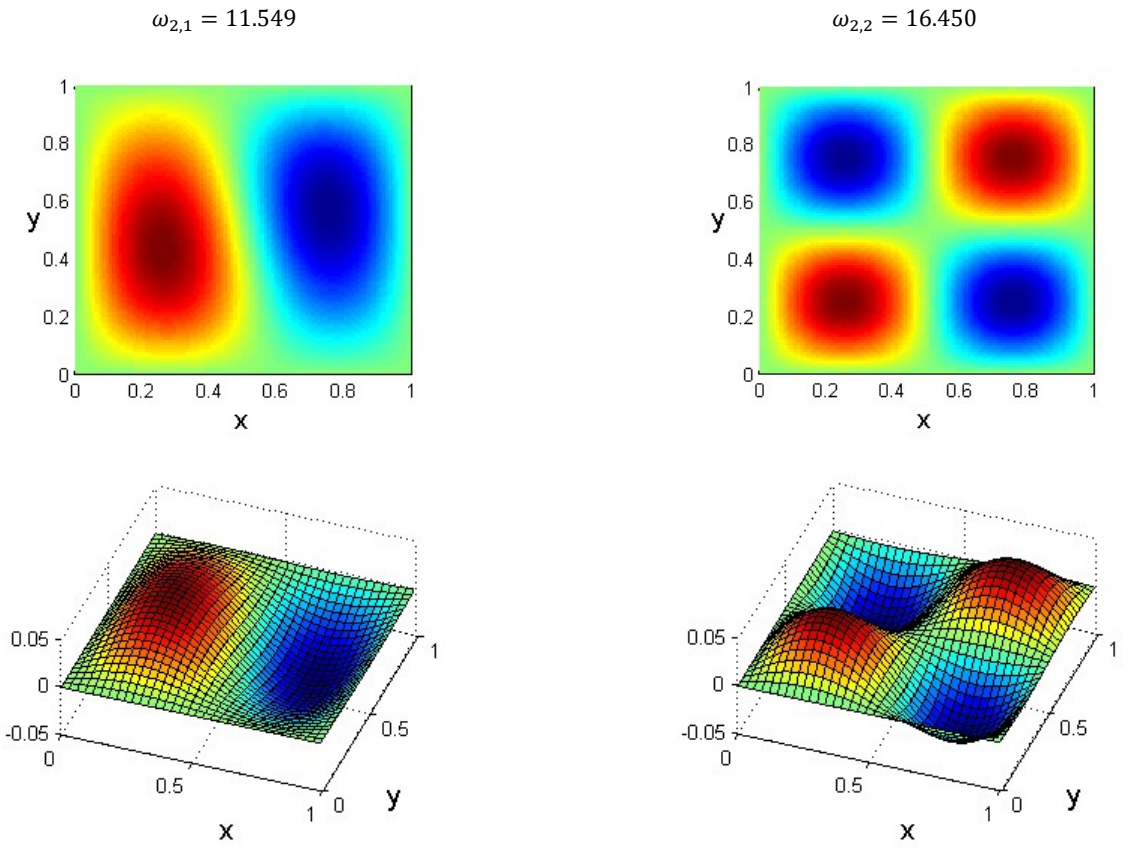

Fig. 10. Dimensionless flexural mode natural frequencies $\omega_{2,1}$ y $\omega_{2,2}$ of square FG plate (Al/ZrO2) ($a = b, a/h = 5$ & $p = 1$).

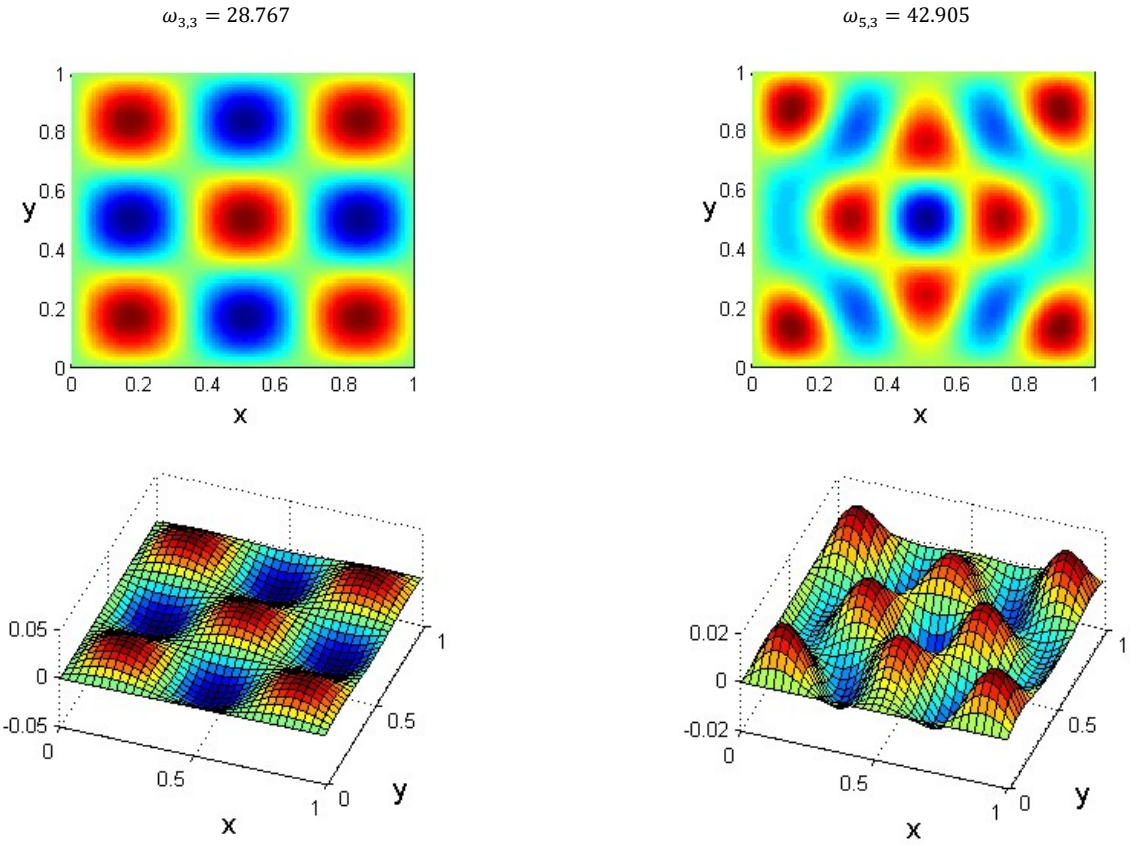

Fig. 11. Dimensionless flexural mode natural frequencies $\omega_{3,3}$ y $\omega_{5,3}$ of square FG plate (Al/ZrO2) ($a = b, a/h = 5$ & $p = 1$).

Table 12. Comparison of non-dimensional flexural natural frequencies for a FG (Al/ZrO_2) square plate ($N = 2, a = b, a/h = 4$).

Theory	$\omega_{1,1}$	$\omega_{1,2}$	$\omega_{1,3}$	$\omega_{2,2}$	$\omega_{2,3}$	$\omega_{3,3}$	$\omega_{4,3}$	$\omega_{5,3}$
$a/h = 4\ p = 1$								
Matsunaga [12]	**5.4276**	---	---	**16.413**	---	---	---	**42.499**
Poly (N=5)	**5.4276**	**11.533**	**19.250**	**16.413**	**23.070**	**28.618**	**35.241**	**42.499**
F1* (N=2)	5.4305	11.549	19.305	16.450	23.157	28.767	35.493	42.905
Err % F1	0.0534	---	---	0.2254	---	---	---	0.9553
F2* (N=2)	5.4332	11.556	19.326	16.467	23.183	28.800	35.534	42.948
Err % F2	0.1032	---	---	0.3290	---	---	---	1.0565
F3* (N=2)	5.4319	11.552	19.309	16.454	23.162	28.772	35.498	42.906
Err % F3	0.0792	---	---	0.2498	---	---	---	0.9577
$a/h = 4\ p = 1$								
Vel [6]	**5.1984**	---	---	**15.611**	---	---	---	**40.206**
Poly (N=5)	**5.1952**	**10.990**	**18.278**	**15.602**	**21.879**	**27.105**	**33.344**	**40.189**
F1* (N=2)	5.2000	11.012	18.345	15.649	21.979	27.267	33.606	40.589
Err % F1	0.0308	---	---	0.2434	---	---	---	0.9526
F2* (N=2)	5.2022	11.019	18.357	15.661	21.994	27.284	33.619	40.591
Err % F2	0.0731	---	---	0.3203	---	---	---	0.9576
F3* (N=2)	5.2007	11.014	18.346	15.651	21.980	27.268	33.604	40.583
Err % F3	0.0442	---	---	0.2562	---	---	---	0.9377

*Optimization 4th.

5. Conclusions

This study presents the bending and free vibration behavior of advanced composite plates via optimized higher order theories with non-polynomial SSSFs. Based on the results, it can be concluded that the accurate free vibration analysis of FG plates can be addressed by the displacement fields with expansion order N=3 as presented in this study. Additionally, the first five natural frequencies can be successfully estimated employing an expansion order, N=2. On the other hand, it is important to notice that the available benchmark examples in the literature use higher order expansion than those proposed in the present study.

The above-mentioned conclusion suggest that is possible to reduce the expansion order of the displacement field without affecting the accuracy of the results. Therefore, an optimization process of the non-polynomial SSSFs' arguments is important and should be further explored.

Acknowledgement

The first author would like to thank D+Imac Lab for the support during the research activity carried out in this paper.

Conflict of Interest

The authors declare no conflict of interest.

Nomenclature

SSSF	Shear strain shape function	ESL	Equivalent single-layer
FGM	Functionally graded material	CUF	Carrera Unified Formulation
FSDT	First order shear deformation theory	RMVT	Reissner mixed variational theorem
TSDT	Third order shear deformation theory	HSDT	High-order shear deformation theory
CPT	Classic plate theory	PVD	Principle of virtual displacements
SSDT	Shear deformation plate theory	FEM	Finite element method

References

[1] Bever MB, Duwez PE. Gradients in composite materials. *Mater Sci Eng* 10 (1972) 1–8.
[2] Miyamoto Y, Kaysser WA, Rabin BH, Kawasaki A, Ford RG. *Functionally graded materials: design, processing and applications*. Kluwer Academic Publishers; 1999.
[3] Kieback B, Neubrand A, Riedel H. Processing techniques for functionally graded materials. *Materials Science and Engineering A* 362 (2003) 81–105.
[4] Swaminathan K, Naveenkumar DT, Zenkour AM, Carrera E. Stress, vibration and buckling analyses of FGM plates - A state-of-the-art review. *Composite Structures* 120 (2015) 10–31.
[5] Reddy JN, Cheng ZQ. Frequency of functionally graded plates with three-dimensional asymptotic approach. *J. Eng. Mech.* 129(18) (2003) 896–900.
[6] Vel SS, Batra RC. Vel SS, Batra RC. Three-dimensional exact solution for the vibration of functionally graded rectangular plates. *J. Sound Vib.* 272 (2004) 703–30.

[7] Mori T, Tanaka K. Average stress in matrix and average elastic energy of materials with misfitting inclusions. *Acta Metall*. 21 (1973) 571–4.
[8] Benveniste Y. A new approach to the application of Mori–Tanaka's theory of composite materials, *Mechanics of Materials* 6 (1987) 147–157.
[9] Zenkour AM. On vibration of functionally graded plates according to a refined trigonometric plate theory. *International Journal of Structural Stability and Dynamics* 5(2) (2005) 279–297.
[10] Zenkour AM. A comprehensive analysis of functionally graded sandwich plates: part 1 – Deflection and stresses. *Int J. Solids Struct*. 42 (2005) 5224–42.
[11] Zenkour AM. A comprehensive analysis of functionally graded sandwich plates: part 2 – buckling and free vibration. *Int. J. Solids Struct*. 42(18–19) (2005) 5243–58.
[12] Matsunaga H. Free vibration and stability of functionally graded plates according to a 2-D higher-order deformation theory. *Compos. Struct.* 82 (2008) 499–512.
[13] Fares ME, Elmarghany MK, Atta D. An efficient and simple refined theory for bending and vibration of functionally graded plates. *Compos. Struct.* 91(3) (2009) 296–305.
[14] Cinefra M, Belouettar S, Soave M, Carrera E. Variable kinematic models applied to free-vibration analysis of functionally graded material shells. *Eur. J. Mech. – A/Solids* 29(6) (2010) 1078–87.
[15] Hadji L, Atmane HA, Tounsi A, Mechab I, Bedia EAA. Free vibration of functionally graded sandwich plates using four-variable refined plate theory. *Appl. Math. Mech. – Engl. Ed*. 32(7) (2011) 925–42.
[16] Qian LF, Batra RC, Chen LM. Free and forced vibrations of thick rectangular plates by using higher-order shear and normal deformable plate theory and meshless local Petrov–Galerkin (MLPG) method. *Comput. Model. Eng. Sci.* 4(5) (2003) 519–34.
[17] Ferreira AJM, Batra RC, Roque CMC, Qian LF, Jorge RMN. Natural frequencies of functionally graded plates by a meshless method. *Compos. Struct.* 75(1-4) (2006) 593–600.
[18] Neves AMA, Ferreira AJM, Carrera E, Cinefra M, Roque CMC., Jorge RMN, Soares CMM. A quasi-3D sinusoidal shear deformation theory for the static and free vibration analysis of functionally graded plates. *Composites: Part B* 43 (2012) 711-725.
[19] Neves AMA, Ferreira AJM, Carrera E, Cinefra M, Roque CMC., Jorge RMN, Soares CMM. Static, free vibration and buckling analysis of isotropic and sandwich functionally graded plates using a quasi-3D higher-order shear deformation theory and a meshless technique. *Composites: Part B* 44 (2013) 657-674.
[20] Carrera E, Brischetto S, Robaldo A. Variable Kinematic Model for the Analysis of Functionally Graded Material Plates. *AIAA Journal* 46(1) (2008) 194-203.
[21] Brischetto S, Carrera E. Advanced mixed theories for bending analysis of functionally graded plates. *Computers & Structures* 88 (2010) 1474-1483.
[22] Carrera E, Brischetto S, Cinefra M, Soave M. Effects of thickness stretching in functionally graded plates and shells. *Compos. Part B Eng.* 42(2) (2011) 123–33.
[23] Mantari JL, Oktem AS, Soares CG. Bending response of functionally graded plates by using a new higher order shear deformation theory. *Compos. Struct.* 94 (2012) 714–23.
[24] Mantari JL, Soares CG. Bending analysis of thick exponentially graded plates using a new trigonometric higher order shear deformation theory. *Compos. Struct.* 94 (2012) 1991–2000.
[25] Mantari JL, Soares CG. A novel higher-order shear deformation theory with stretching effect for functionally graded plates. *Compos. Part B Eng.* 45(1) (2013) 268–81.
[26] Mantari JL, Soares CG. Optimized sinusoidal higher order shear deformation theory for the analysis of functionally graded plates and shells. *Compos. Part B Eng.* 56 (2014) 126–36.
[27] Ait Amar Meziane, Abdelaziz HH, Tounsi A. An efficient and simple refined theory for buckling and free vibration of exponentially graded sandwich plates under various boundary conditions. *J. Sandw. Struct. Mater.* 16(3) (2014) 293-318.
[28] Abdelaziz HH, Ait Amar Meziane, Bousahla AA, Alwabli AS. An efficient hyperbolic shear deformation theory for bending, buckling and free vibration of FGM sandwich plates with various boundary conditions. *Steel and Composite Structures* 25(6) (2017) 693-704.